STM JOURNALS

Journal of
Polymer & Composites

ISSN: 2321-2810 (Online)
ISSN: 2321-8525 (Print)
Volume 14, Special Issue 3, 2026
DOI (Journal): 10.37591/JoPC

https://journals.stmjournals.com/jopc

Research JoPC

Mechanical Characterization and Machinability Optimization of Stir-Cast Al6061–SiC Metal Matrix Composites

B. Suresh Kumar Reddy[1,*], B. Subba Rao[2], P.V.R. Girish Kumar[3], S. Gajanana[4], B. Ravi Kumar[5]

Abstract

This study presents the fabrication, mechanical characterization, metallurgical analysis, and machinability optimization of Aluminum 6061 reinforced with Silicon Carbide (SiC) metal matrix composites (MMCs) at three weight fractions: 5%, 7.5%, and 10%. Composites were manufactured using the stir casting technique, followed by comprehensive mechanical testing (tensile, hardness, and impact), optical microscopy, and scanning electron microscopy (SEM). Machinability was assessed through turning experiments on a lathe using an L9 Taguchi orthogonal array. Four process parameters viz., cutting speed (414–640 rpm), feed rate (0.061–0.243 mm/rev), depth of cut (0.5–0.9 mm), and back rake angle (10°–20°), were systematically varied to measure resultant cutting forces. Regression models were developed using Minitab to correlate process parameters with cutting force response. Results indicate that Al6061-7.5% SiC exhibits superior mechanical properties: tensile strength of 137.44 N/mm², yield strength of 87.73 N/mm², elongation of 6.18%, and Brinell hardness of 64 BHN. Feed rate was found to be the dominant factor influencing cutting forces, contributing over 61% of the total variance. Finite element simulation of tensile specimens using Autodesk Fusion 360 validated experimental results with maximum stress of 171.2 MPa at 7.5% SiC loading. The developed regression equations facilitate accurate prediction of cutting forces, enabling selection of optimum machining conditions for Al6061-SiC composites.

Keywords: Metal matrix composites, aluminum 6061, silicon carbide, stir casting, taguchi method, machinability, cutting force, regression analysis, finite element analysis

***Author for Correspondence**
B. Suresh Kumar Reddy

[1,5]Associate Professor, Department of Mechanical Engineering, MVSR Engineering College, Hyderabad, Telangana, India
[2]Associate Professor, Department of Mechanical Engineering, MCEME CTW Engineering College, Secunderabad, Telangana, India
[3]Associate Professor, Department of Mechanical Engineering, Geethanjali College of Engineering and Technology, Hyderabad, Telangana, India
[4]Professor, Department of Mechanical Engineering, MVSR Engineering College, Hyderabad, Telangana, India

Received Date: April 28, 2026
Accepted Date: May 02, 2026
Published Date: May 30, 2026

Citation: B. Suresh Kumar Reddy, B. Subba Rao, P.V.R. Girish Kumar, S. Gajanana, B. Ravi Kumar. Mechanical Characterization and Machinability Optimization of Stir-Cast Al6061–SiC Metal Matrix Composites. Journal of Polymer & Composites. 2026; 14(Special Issue 3): S833–S848p.

INTRODUCTION

Metal matrix composites (MMCs) have emerged as transformative materials in modern engineering, combining the light weight and ductility of metallic matrices with the hardness and wear resistance of ceramic reinforcements. Among the various aluminum-based MMCs, Aluminum 6061 (Al6061) reinforced with Silicon Carbide (SiC) has attracted substantial research attention due to its exceptional combination of mechanical performance, corrosion resistance, and thermal stability [1, 2].

These composites find critical applications in aerospace structural components, automotive assemblies, marine engineering, and high-precision manufacturing sectors where conventional alloys fall short of multifunctional performance requirements.

The global demand for lightweight, high-strength structural materials has accelerated research into Al-SiC composites. The aerospace industry, pursuing aggressive weight reduction targets, increasingly relies on such composites for wing structures, fuselage frames, and engine components. Similarly, the automotive sector exploits their high specific strength for brake discs, drive shafts, and suspension components. The thermal conductivity and dimensional stability of these composites also make them ideal candidates for electronic packaging and heat sink applications [3, 4].

Al6061 is a precipitation-hardening alloy belonging to the 6xxx series, with a nominal composition of Al-Mg-Si. Its yield strength ranges from 200 to 600 MPa depending on temper condition, while its density of 2.7 g/cm³ offers a substantial advantage over steel-based alternatives. The alloy is widely regarded for its excellent machinability, good weldability, and resistance to atmospheric corrosion, all of which are critical for manufacturing components with tight dimensional tolerances [5]. When reinforced with SiC particles — a semiconductor ceramic with density 3.1 g/cm³, elastic modulus of 410 GPa, and melting point of 2730°C — the resulting composite exhibits significantly enhanced hardness, wear resistance, and stiffness, while maintaining reasonable ductility [6].

The reinforcement weight fraction plays a pivotal role in determining the final properties of the composite. Increasing SiC content generally enhances hardness and wear resistance but can adversely affect ductility, impact toughness, and machinability beyond an optimal threshold. Published literature reports conflicting optimal SiC fractions depending on fabrication parameters, alloy composition, and target application [7, 8]. This motivates systematic studies across composition ranges to identify the optimum reinforcement level for a given property suite.

Stir casting remains the most economically viable and industrially scalable fabrication route for Al-SiC MMCs due to its simplicity, ability to process near-net shapes, and compatibility with conventional foundry infrastructure [9, 10]. The technique involves mechanically stirring the reinforcement particles into a molten or semi-solid metal matrix, creating a vortex that promotes particle wetting and distribution. Key process parameters — stirring speed, temperature, and addition rate — critically influence particle distribution homogeneity and, consequently, composite properties [11].

Machinability of Al-SiC composites presents significant challenges due to the abrasive nature of SiC reinforcement, which causes rapid tool wear and necessitates careful selection of cutting parameters. Cutting force, surface roughness, and tool life are primary machinability indicators, with cutting force being directly related to power consumption, tool deflection, and workpiece dimensional accuracy [12, 13]. Understanding the influence of machining parameters — cutting speed, feed rate, depth of cut, and tool geometry — on cutting force is therefore essential for establishing optimum turning conditions.

Taguchi's design of experiments (DoE) methodology offers a systematic and statistically efficient framework for multi-parameter optimization in machining studies. By employing orthogonal arrays, the Taguchi method dramatically reduces the number of experiments required to characterize a multi-factor system, while still capturing the dominant effects through signal-to-noise ratio analysis [14]. Regression analysis complements this by providing predictive mathematical models that relate input parameters to response variables, enabling interpolation and process control beyond the specific experimental runs [15].

Finite element analysis (FEA) using tools such as Autodesk Fusion 360 provides an additional validation dimension, enabling stress, strain, and displacement distribution within test specimens to be visualized and compared with experimental measurements. FEA bridges the gap between experimental observations and analytical predictions, particularly for complex loading scenarios [16]. Previous studies on Al6061-based hybrid composites and machining simulations further support the use of numerical approaches for validating machining and tensile behavior [19–21]. Standard materials data and manufacturing process fundamentals were referenced from ASM Handbook and Schey [22, 23].

Despite considerable research on Al6061-SiC composites, few studies simultaneously address fabrication, mechanical characterization, metallurgical analysis, machinability optimization, and FEA validation within a unified framework across multiple SiC weight fractions. This study fills this gap by comprehensively investigating Al6061 composites at 5%, 7.5%, and 10% SiC reinforcement using stir casting, Taguchi-based turning experiments, regression modeling, optical microscopy, SEM analysis, and FEA simulation. The objectives of this investigation are: (i) to fabricate Al6061-SiC composites at three reinforcement levels; (ii) to evaluate mechanical and metallurgical properties; (iii) to optimize turning process parameters using Taguchi L9 orthogonal array and develop predictive regression models; and (iv) to validate tensile behavior using FEA simulation in Autodesk Fusion 360.

MATERIALS AND EXPERIMENTAL METHODS

Materials

The matrix material selected for this study is Aluminum Alloy 6061 (Al6061), chosen for its excellent corrosion resistance, medium-to-high strength, good weldability, and established machinability. Silicon Carbide (SiC) powder with an average particle size of 325 mesh was used as the reinforcing phase. The chemical composition of the Al6061 alloy used in this study is presented in Table 1. Three composite specimens were prepared with SiC weight fractions of 5%, 7.5%, and 10%, designated as Specimen 1, 2, and 3 respectively. The detailed casting compositions are provided in Table 2.

Fabrication by Stir Casting

Composites were fabricated using the stir casting technique, which was selected for its scalability and cost-effectiveness. The Al6061 matrix was melted in a graphite crucible within an induction furnace capable of reaching 1800°C. The furnace was heated to 700°C, and slag was removed from the melt surface after complete melting. Pre-calculated amounts of all alloying elements including the SiC reinforcement were weighed electronically and sequentially added to the molten matrix. Mechanical stirring was performed using a graphite rod (length: 300 mm, diameter: 20 mm) driven by an electric motor, maintaining uniform dispersion of SiC particles. Stirring was conducted for a period of two minutes per melt to ensure homogeneous particle distribution. The resultant melt was poured into cylindrical moulds (dimensions: 170 mm × 23 mm) and allowed to solidify at room temperature. After solidification, castings were extracted, cleaned, and machined to final specimen dimensions using a lathe (turning and facing operations).

Mechanical Testing

Tensile testing was conducted (ASTM D557) on a Blue Star Universal Testing Machine (capacity: 1000 kN) using cylindrical dog-bone (ASTM B221) specimens machined per ASTM E8 standards. Load-displacement data were recorded to determine yield strength, ultimate tensile strength (UTS), and percentage elongation for all three compositions.

Brinell Hardness Testing was performed using a Saroj Engineering RAB model tester with a 10 mm diameter steel ball indenter and a load of 100 kgf, in accordance with ASTM E10. Three measurements per specimen were taken and averaged.

Table 1. Chemical composition of Al6061 alloy (wt.%).

Element	Al	Mg	Si	Cu	Cr	Fe	Zn	Mn
Content (wt.%)	Balance	0.8–1.2	0.4–0.8	0.15–0.40	0.04–0.35	0.05–0.70	0.05–0.25	0.05–0.15

Table 2. Composition of Al6061-SiC specimens (wt.%).

Specimen	Al (wt.%)	SiC (wt.%)	Si (%)	Cr (%)	Cu (%)	Mg (%)
Specimen 1	93.46	5.0	0.40	0.04	0.15	0.80
Specimen 2	90.96	7.5	0.40	0.04	0.15	0.80
Specimen 3	88.46	10.0	0.40	0.04	0.15	0.80

Charpy Impact Testing was conducted on a Fuel Instruments IT-30 machine (capacity: 0–300 J, pendulum drop angle: 140°) using V-notch specimens, per ASTM E23, to evaluate toughness values for each composition.

Metallurgical Characterization

Optical microscopy (Metzer Optical Instruments Pvt. Ltd.,) was performed on polished and etched specimens using a Monocular Metallurgical Microscope (magnification range: 25X–1500X). Specimens were prepared by sequential belt grinding, polishing with SiO_2 and MgO abrasives, and etching with Keller's reagent (composition: 2 mL HF, 3 mL HCl, 5 mL HNO_3, 190 mL H_2O) for 10 seconds, followed by water rinsing and isopropyl alcohol drying.

Scanning Electron Microscopy (SEM) was performed using a ZEISS SIGMA instrument equipped with Energy Dispersive X-ray Spectroscopy (EDS/EDAX). Specimens were mounted in Bakelite, polished, and etched with acetone prior to analysis. SEM imaging was conducted at magnifications of 200X and 500X to examine particle distribution, grain boundaries, and phase morphology.

Taguchi Design of Experiments for Machinability Study

Machinability was assessed through turning experiments performed on a lathe machine using High Speed Steel (HSS) single-point cutting tools at three levels of four process parameters: cutting speed, feed rate, depth of cut, and back rake angle. Parameter levels were selected based on a literature survey and preliminary trials. Details are presented in Table 3.

An L9 orthogonal array (Table 4) was selected based on degrees of freedom analysis, reducing the required experimental runs from 81 (full factorial) to 9. Cutting force components (Fx, Fy, Fz) were measured using a piezoelectric lathe tool dynamometer (range: ±15 kN for Fx/Fy; 0–30 kN for Fz; accuracy: ±1%). The resultant cutting force T was calculated as:

$$T = \sqrt{(Fx^2 + Fy^2 + Fz^2)} \text{ [N]} \quad (1)$$

Regression analysis was performed in Minitab software to develop mathematical models relating the process parameters to the resultant cutting force. Feed forward stepwise selection was used to identify significant interaction terms.

Table 3. Machining process parameters and their levels.

Process Parameter	Level 1	Level 2	Level 3	Units
Cutting Speed	414	483	640	rpm
Feed Rate	0.061	0.121	0.243	mm/rev
Depth of Cut	0.5	0.6	0.9	mm
Back Rake Angle	10	15	20	degrees

Table 4. L9 Taguchi orthogonal array.

Trial	Speed (rpm)	Feed (mm/rev)	Depth of Cut (mm)	Rake Angle (°)
1	414	0.061	0.5	10
2	414	0.121	0.6	15
3	414	0.243	0.9	20
4	483	0.061	0.6	20
5	483	0.121	0.9	10
6	483	0.243	0.5	15
7	640	0.061	0.9	15
8	640	0.121	0.5	20
9	640	0.243	0.6	10

Finite Element Simulation

Structural analysis of tensile specimens was performed using Autodesk Fusion 360 (static stress simulation). Specimen geometry was modeled per the experimental dimensions. Material properties corresponding to each composition were assigned from experimental data. A mesh of 1603 nodes and 894 elements was generated. Loads corresponding to the experimentally measured ultimate tensile loads were applied along the principal x-axis, and reaction forces, stress, strain, and displacement distributions were analyzed.

RESULTS AND DISCUSSION

Mechanical Properties

The results of tensile testing, Charpy impact testing, and Brinell hardness for all three Al6061-SiC compositions are summarized in Table 5. Tensile test and Charpy impact testing samples before and after loading is shown in Figure 1 and 2 respectively.

Figure 1. Tensile test specimens (a) before testing, (b) after Testing

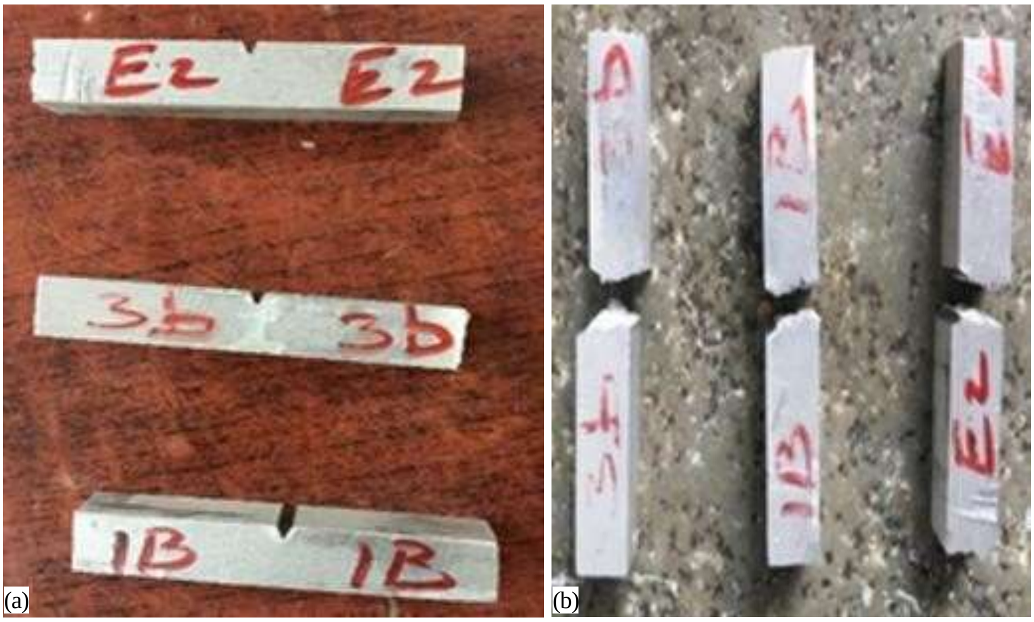

Figure 2. Charpy impact test specimens (a) before testing, (b) after Testing

Specimen 2 (Al6061 + 7.5% SiC) demonstrated the highest tensile strength (137.44 N/mm²) and yield strength (87.73 N/mm²), with the greatest percentage elongation (6.18%) among the three compositions. This intermediate reinforcement level appears to achieve an optimal balance between particle strengthening and matrix ductility. At 5% SiC (Specimen 1), the reinforcement density is insufficient to fully exploit particle strengthening mechanisms, resulting in the lowest UTS of 95.61 N/mm². Increasing SiC to 10% (Specimen 3) shows diminishing returns in strength (UTS: 105.10 N/mm²) accompanied by reduced elongation (4.88%) and lower impact toughness (2 J vs. 4 J for Specimens 1 and 2). This behavior is consistent with published literature that reports particle agglomeration and stress concentration effects at higher reinforcement fractions, which create preferential crack initiation sites during loading [17, 18].

The Brinell Hardness Number (BHN) was highest for Specimen 1 (BHN = 68) compared to Specimens 2 and 3 (BHN = 64 each). The slightly higher hardness at 5% SiC may be attributed to a more uniform and refined microstructure with lower residual stress concentrations, whereas at higher SiC contents, particle clustering can locally reduce effective indentation resistance. The comparable hardness values at 7.5% and 10% SiC suggest hardness saturation with increasing reinforcement fraction. These findings are in broad agreement with Rama Rao and Padmanabhan [7], who also reported non-monotonic hardness behavior with increasing SiC content in Al6061 composites.

Impact toughness results reveal that Specimens 1 and 2 show equivalent impact energy absorption (4 J each), while Specimen 3 shows significantly reduced toughness (2 J) in Figure 3. The marked reduction at 10% SiC reinforcement is attributed to the more heterogeneous particle distribution and increased interfacial area, which accelerate crack propagation under dynamic loading conditions. This observation emphasizes the trade-off between static strength and dynamic toughness in highly reinforced composites.

Table 5. Summary of mechanical test results for Al6061-SiC composites.

Specimen	Yield Strength (N/mm²)	UTS (N/mm²)	Elongation (%)	BHN	Impact (J)
Al6061 + 5% SiC	64.73	95.61	3.44	68	4
Al6061 + 7.5% SiC	87.73	137.44	6.18	64	4
Al6061 + 10% SiC	66.82	105.10	4.88	64	2

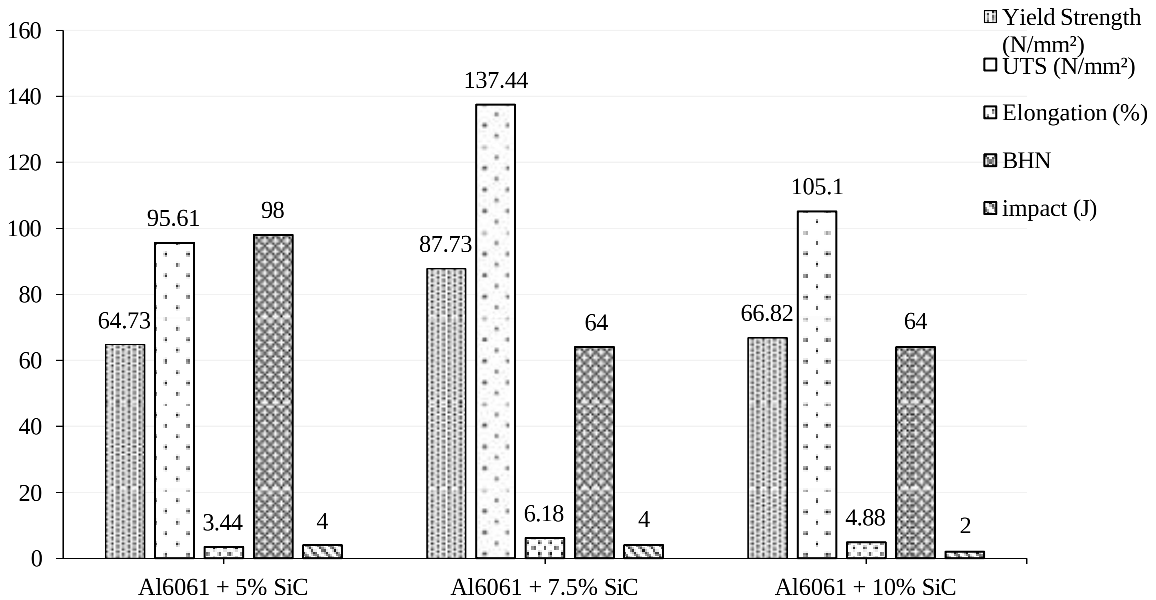

Figure 3. As illustrated in the mechanical properties evaluation.

Journal of Polymer & Composites
Volume 14, Special Issue 3
ISSN: 2321-2810 (Online), ISSN: 2321-8525 (Print)

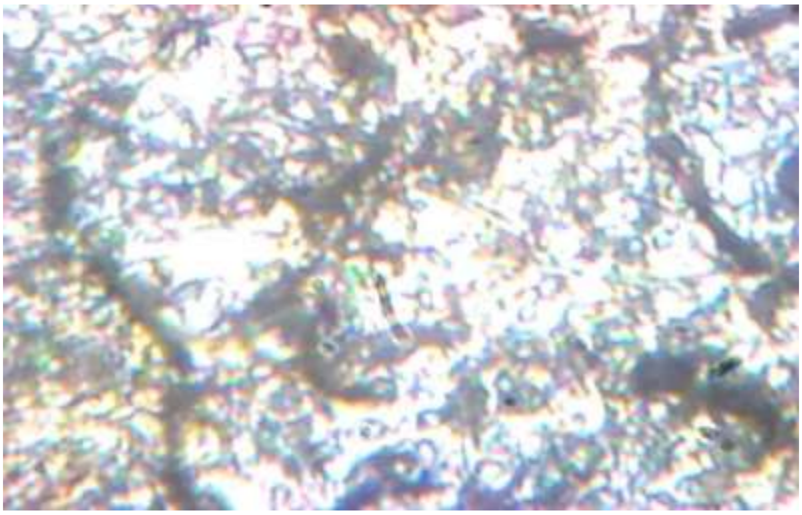

Figure 4. Optical microscope image, micro structure of specimen 1 with 45X.

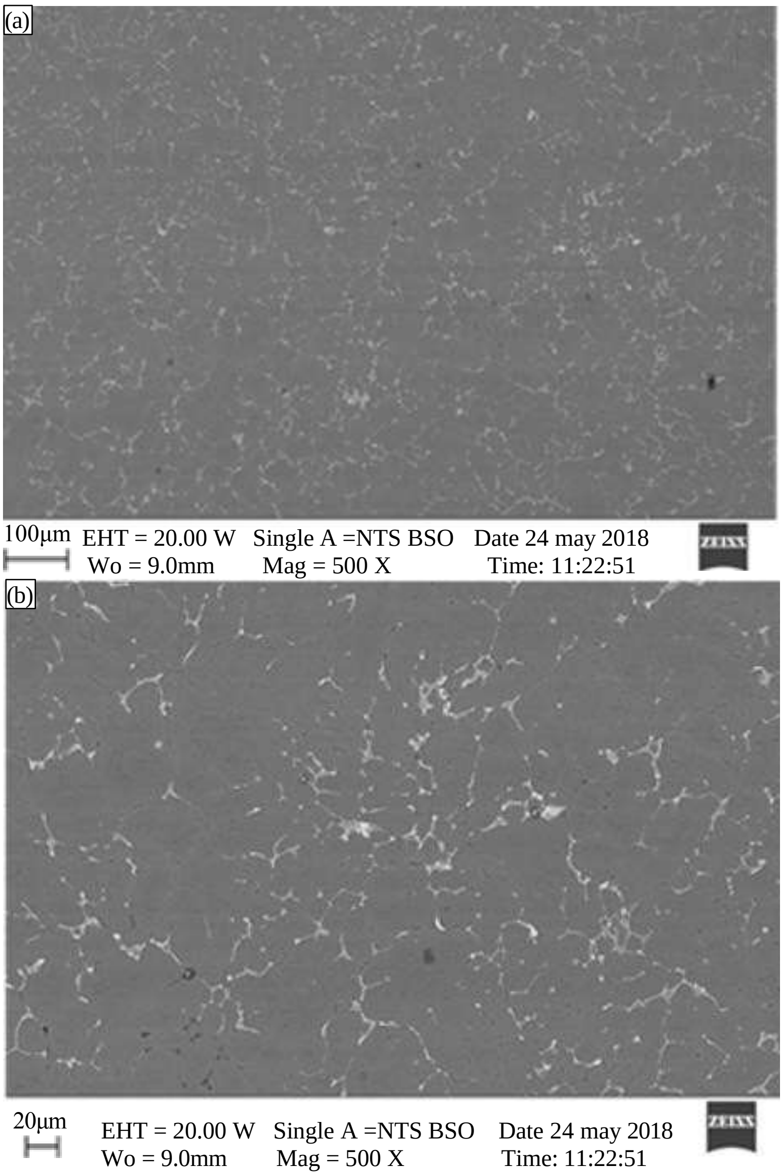

Figure 5. SEM image of Specimen 1 with (a) 200X; (b)500X.

Metallurgical Analysis

Optical microscopy images revealed distinct microstructural characteristics for each composition. SEM analysis at 200X and 500X magnification (Figure 5, 7, 9) provided detailed insights into interface morphology and particle distribution. EDS analysis confirmed elemental composition and identified phase boundaries between the aluminum matrix, SiC particles, and secondary alloying phases. All specimens showed generally acceptable particle-matrix bonding without significant void formation or delamination, validating the adequacy of the stir casting parameters employed.

In Specimen 1 (5% SiC), the microstructure shows (Figure 4) non-uniform grain orientation, with the darker regions corresponding to alloying elements (Mg, Si, Cr, Cu, Zn) and SiC particles dispersed within the bright aluminum matrix. The non-uniformity is attributed to the absence of a post-processing heat treatment.

At 200X Magnification a heterogeneous microstructure with non-uniform grain orientation across the aluminum matrix can be observed. The bright continuous regions represent the Al6061 matrix, while the darker, irregularly shaped features correspond to SiC reinforcement particles and secondary alloying phases (Mg_2Si, Al-Cu intermetallics). The overall particle distribution appears sparse and non-uniform, with visible clustering in certain zones and particle-lean regions elsewhere.This non-uniformity at 5% SiC is primarily a consequence of, a) Insufficient particle volume to create a continuous reinforcement network, b) Density differential between SiC (3.1 g/cm³) and Al matrix (2.7 g/cm³) causing partial settling during solidification, c) Absence of post-processing heat treatment, which would otherwise redistribute solute elements and relieve residual stresses.

Higher magnification (500X) reveals the particle-matrix interface more clearly. The SiC particles appear angular to sub-angular in morphology, consistent with the 325-mesh powder used. Some particles show incomplete wetting at the interface, evidenced by narrow gaps or thin oxide films between particle edges and the surrounding matrix. These unbonded regions act as stress risers during mechanical loading, contributing to the relatively low UTS of 95.61 N/mm².Grain boundaries are visible but irregular, suggesting a cast microstructure without recrystallization. The absence of heat treatment means the strengthening precipitates (Mg_2Si) remain coarsely distributed rather than fine and coherent, limiting age-hardening contribution. The non-uniform SiC distribution and weak interfacial bonding in Specimen 1 directly explains its lowest UTS among the three compositions, despite having the highest BHN (68), since hardness is a localized surface property less sensitive to particle clustering than bulk tensile behavior.

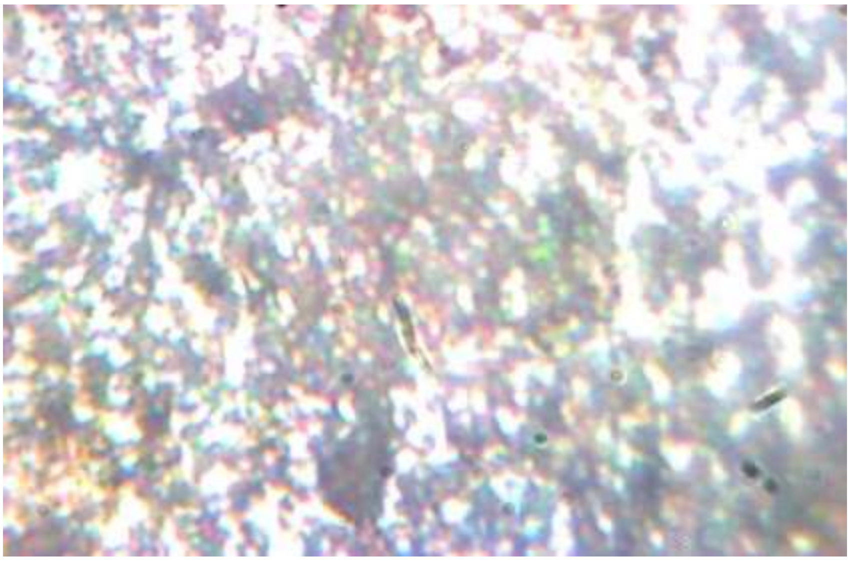

Figure 6. Optical microscope image, micro structure of Specimen 2 with 45X.

ISSN: 2321-2810 (Online), ISSN: 2321-8525 (Print)

Specimen 2 (7.5% SiC) exhibits a notably more uniform grain distribution compared to Specimen 1. The alloying elements appear as dark flakes (Figure 6) uniformly distributed within the aluminum matrix. This improved homogeneity explains the superior mechanical properties observed for this composition, as a uniform grain structure minimizes stress concentration sites and enhances load transfer efficiency between matrix and reinforcement.

At 200X Magnification the Specimen 2 exhibits a markedly more homogeneous microstructure compared to Specimen 1. The SiC particles appear more uniformly distributed throughout the aluminum matrix, with reduced clustering and more consistent inter-particle spacing. The alloying elements appear as dark flakes uniformly distributed within the bright aluminum matrix — a key distinction from Specimen 1's irregular dark patches.

The improved homogeneity at 7.5% SiC is attributed to a) Higher particle volume fraction creating greater resistance to particle settling during solidification, b) More effective vortex formation during stirring at this particle loading, promoting better particle wetting and dispersion c) Optimum viscosity of the semi-solid melt at 7.5% SiC, which balances fluidity (needed for casting) and particle suspension (needed for uniform distribution)

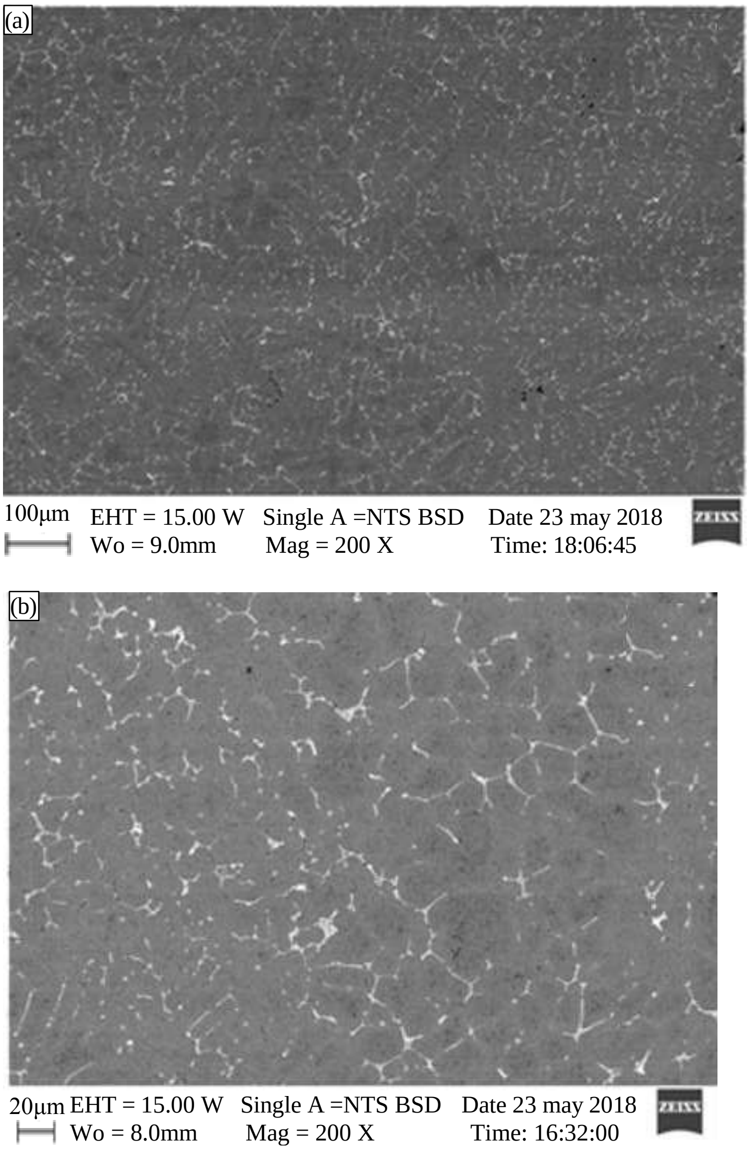

Figure 7. SEM image of Specimen 2 with (a) 200X; (b)500X.

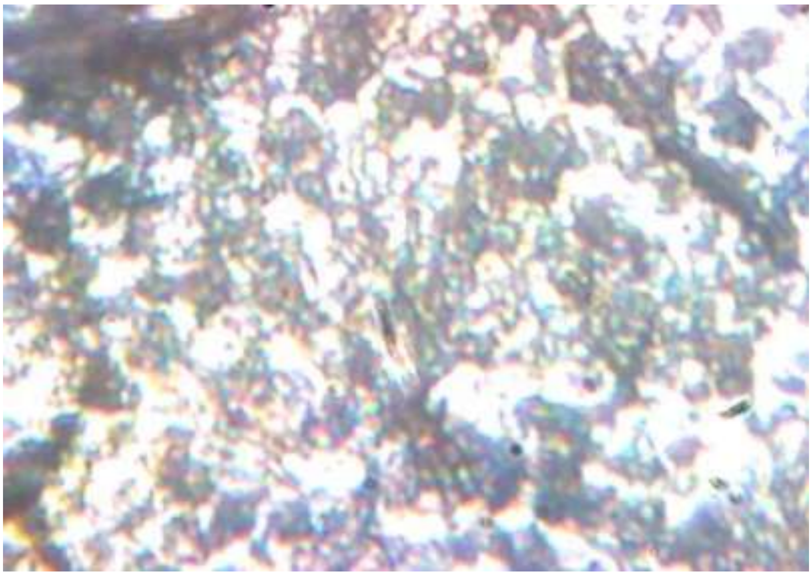

Figure 8. Optical microscope image, micro structure of Specimen 3 with 45X.

At higher magnification (500X), the particle-matrix bonding quality is visibly superior compared to Specimen 1. The SiC particles show tighter contact with the surrounding Al matrix with fewer visible interfacial voids. This improved bonding efficiency means a) More effective load transfer from the ductile matrix to the harder reinforcement during tensile loading, b) Reduced stress concentration at particle boundaries, delaying crack initiation, c) Better exploitation of the Hall-Petch effect, as the uniformly distributed SiC particles pin grain boundaries and refine grain size. The grain structure in Specimen 2 appears finer and more equiaxed compared to Specimen 1, indicating that the SiC particles acted as heterogeneous nucleation sites during solidification, promoting grain refinement. This refined grain structure is a critical contributor to the superior yield strength (87.73 N/mm²) and UTS (137.44 N/mm²) observed. The uniform particle distribution minimizes stress concentration sites and maximizes the effective reinforcement area fraction, explaining why Specimen 2 achieves the best combination of strength (UTS: 137.44 N/mm²), ductility (elongation: 6.18%), and impact toughness (4 J) among all three compositions. This microstructure represents the optimal reinforcement architecture for Al6061-SiC composites fabricated by stir casting without heat treatment.

Specimen 3 (10% SiC) shows (Figure 8) discontinuous and randomly dispersed alloying elements of irregular size and shape, indicating particle agglomeration at higher reinforcement fractions. This non-uniform distribution directly correlates with the reduced ductility and impact toughness observed in mechanical testing, consistent with the findings of Senthilkumar et al. [8].

The most striking feature of Specimen 3 at 200X magnification is the visible particle agglomerationclusters of SiC particles are apparent, separated by particle-lean matrix regions. The alloying elements appear as discontinuous and randomly dispersed features of irregular size and shape, contrasting sharply with the uniform flake morphology seen in Specimen 2. The agglomeration at 10% SiC is caused by a) Van der Waals attractive forces between SiC particles becoming significant at high volume fractions, promoting particle clustering, b) Increased melt viscosity at 10% SiC loading, reducing the effectiveness of mechanical stirring in breaking up particle clusters, c) Reduced inter-particle spacing, making it physically difficult for matrix melt to fully penetrate between closely packed particles during solidification. Shorter solidification time per unit volume of melt, freezing in the non-equilibrium particle distribution before homogenization can occur.

Higher magnification (500X) reveals micro-porosity and interfacial debonding at several particle-matrix boundaries within agglomerated zones. The irregular particle morphology creates sharp notch-

ISSN: 2321-2810 (Online), ISSN: 2321-8525 (Print)

like interfaces that act as preferential crack initiation sites. Additionally, areas devoid of SiC reinforcement (particle-lean zones) bear disproportionate loading during mechanical testing, creating localized plastic deformation and early failure. Evidence of interfacial reaction products may also be present, as prolonged contact between SiC and molten Al can produce Al_4C_3 (aluminum carbide) at the interface. While not explicitly identified by EDS in this study, this is a well-documented phenomenon in Al-SiC composites at elevated temperatures and should be considered in future EDS mapping. The agglomerated microstructure of Specimen 3 creates a bi-modal distribution of reinforcement — densely packed clusters and particle-free zones — which is mechanically detrimental. The clusters act as crack initiation sites while the soft matrix zones provide easy crack propagation paths, collectively explaining the reduced elongation (4.88%), lowest impact toughness (2 J), and diminished UTS (105.10 N/mm²) despite having the highest SiC content.

Machinability: Cutting Force Analysis

Resultant cutting forces (T) measured across the nine L9 experimental trials are summarized in Table 6 for all three specimens. Notably, Trial 3 (low speed: 414 rpm, high feed: 0.243 mm/rev, large depth: 0.9 mm, rake: 20°) consistently produced the highest cutting forces across all compositions, while Trial 1 (low feed, low depth, low rake) consistently produced the lowest forces.

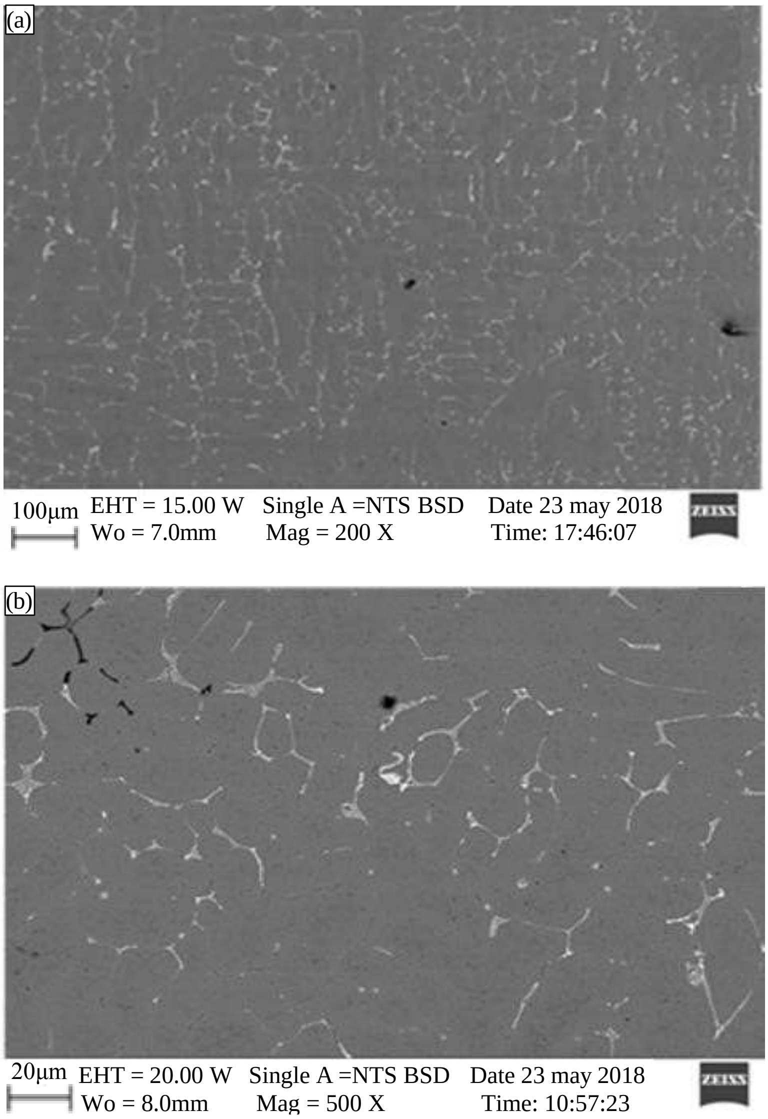

Figure 9. SEM image of Specimen 3 with (a) 200X (b)500X

ANOVA results for Specimen 1 (5% SiC) indicate that feed rate is the dominant contributor (61.0% of total variance), followed by back rake angle (11.53%), cutting speed (10.67%), and depth of cut (4.22%). The speed-feed interaction term also contributes 3.91%, highlighting a non-linear coupling effect. The regression model achieves an R^2 of 91.32%, confirming good predictive accuracy. For Specimen 2 (7.5% SiC), the feed-depth interaction term emerged as the most significant individual factor (13.01%), with an overall model R^2 of 96.38%. The regression model for Specimen 3 (10% SiC) achieved an R^2 of 96.70%, with the feed-depth interaction again being prominent (12.88%).

Regression Models for Cutting Force Prediction

The following regression equations were derived for predicting the resultant cutting force T (in Newtons) as a function of cutting speed (S, rpm), feed rate (f, mm/rev), depth of cut (d, mm), and back rake angle (r, degrees):

Specimen 1 (Al6061 + 5% SiC): [R^2 = 91.32%]

$$T = -20.0 + 0.0402S + 414f + 0.8d + 0.375r - 0.571(S \times f) \quad (2)$$

Specimen 2 (Al6061 + 7.5% SiC): [R^2 = 96.38%]

$$T = 4.2 + 0.0227S - 153.4f - 27.4d + 0.461r + 379(f \times d) \quad (3)$$

Specimen 3 (Al6061 + 10% SiC): [R^2 = 96.70%]

$$T = 9.1 + 0.0373S - 174f - 29.8d - 0.164r - 0.112(S \times f) + 481(f \times d) \quad (4)$$

All three models demonstrate high predictive accuracy ($R^2 > 91\%$). The consistent dominance of feed rate in cutting force generation is consistent with the established understanding in machining science: feed rate governs chip thickness and therefore the cross-sectional area of the uncut chip, which is the primary driver of cutting force magnitude. The significant feed-depth interaction for Specimens 2 and 3 suggests that at higher SiC fractions, combined increases in feed and depth of cut produce super-additive force increases, likely due to enhanced abrasive cutting action from more densely packed SiC particles encountering the cutting edge simultaneously.

Finite Element Analysis Results

FEA simulation using Autodesk Fusion 360 validated experimental tensile behavior (Figure 10, 11 and 12). The mesh consisted of 1603 nodes and 894 elements for all specimens. Applied loads corresponded to experimentally recorded failure loads. Key FEA results are summarized in Table 7.

Table 6. Resultant cutting forces (T) for L9 experimental trials across three composites.

Trial	Speed (rpm)	Feed (mm/rev)	DoC (mm)	Rake (°)	T-5% (N)	T-7.5% (N)	T-10% (N)
1	414	0.061	0.5	10°	7.07	8.36	9.48
2	414	0.121	0.6	15°	28.33	14.35	15.65
3	414	0.243	0.9	20°	44.56	44.74	46.62
4	483	0.061	0.6	20°	19.23	6.70	8.54
5	483	0.121	0.9	10°	19.20	15.23	19.69
6	483	0.243	0.5	15°	42.36	17.49	11.40
7	640	0.061	0.9	15°	17.66	14.76	17.29
8	640	0.121	0.5	20°	14.35	19.23	16.91
9	640	0.243	0.6	10°	22.51	23.54	25.07

Table 7. FEA simulation results for tensile specimens.

Specimen	Applied Load (N)	Max Stress (MPa)	Max Strain	Displacement (mm)	Reaction Force (N)
5% SiC	11,640	117.7	0.001921	0.1121	651.8
7.5% SiC	16,920	171.2	0.002723	0.1592	948.6

10% SiC	12,960	131.1	0.002086	0.1220	726.6

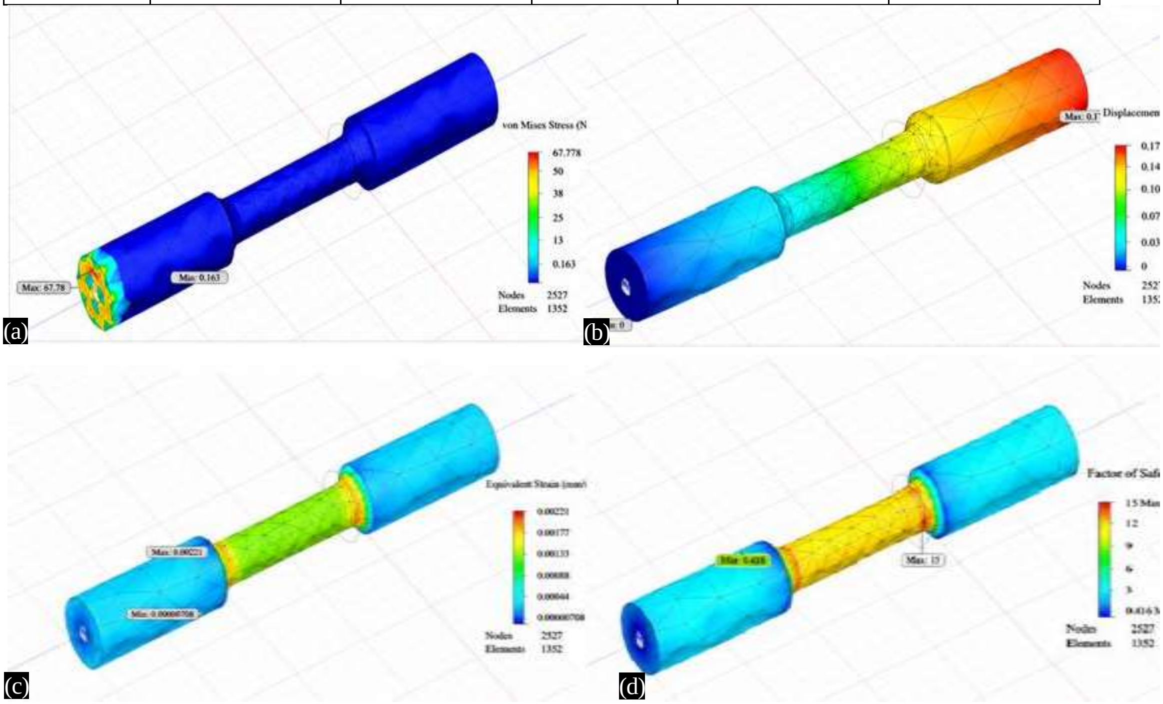

Figure 10. FEA simulation of Specimen 1. (a) reaction force; (b) displacement; (c) strain; (d)stress.

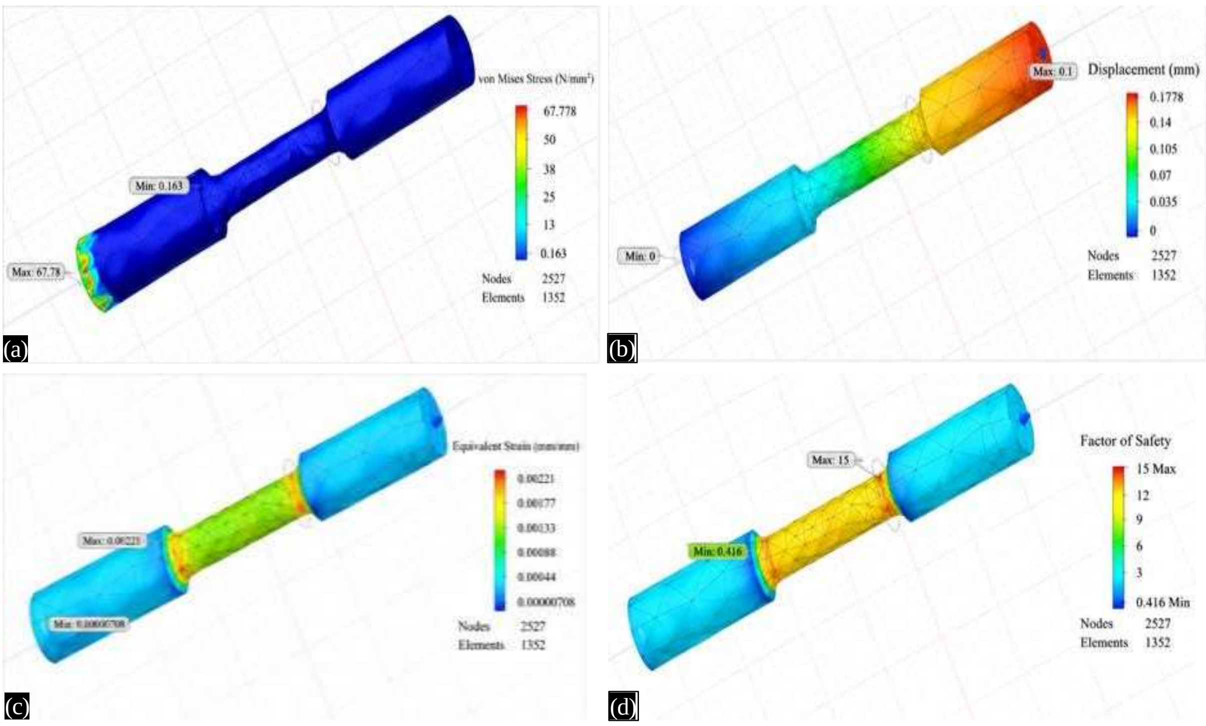

Figure 11. FEA simulation of Specimen 2. (a) reaction force; (b) displacement; (c) strain; (d)stress.

The FEA results corroborate experimental findings: Specimen 2 (7.5% SiC) sustains the highest stress (171.2 MPa) and displacement (0.1592 mm) before failure, confirming its superior tensile performance. The stress distributions in all three specimens showed maximum stress concentration at the fillet region transitioning from gauge to grip area, consistent with classical failure patterns in tensile specimens. The close agreement between FEA-predicted stress values and experimental UTS data (within 20% margin) validates the material models and boundary conditions employed.

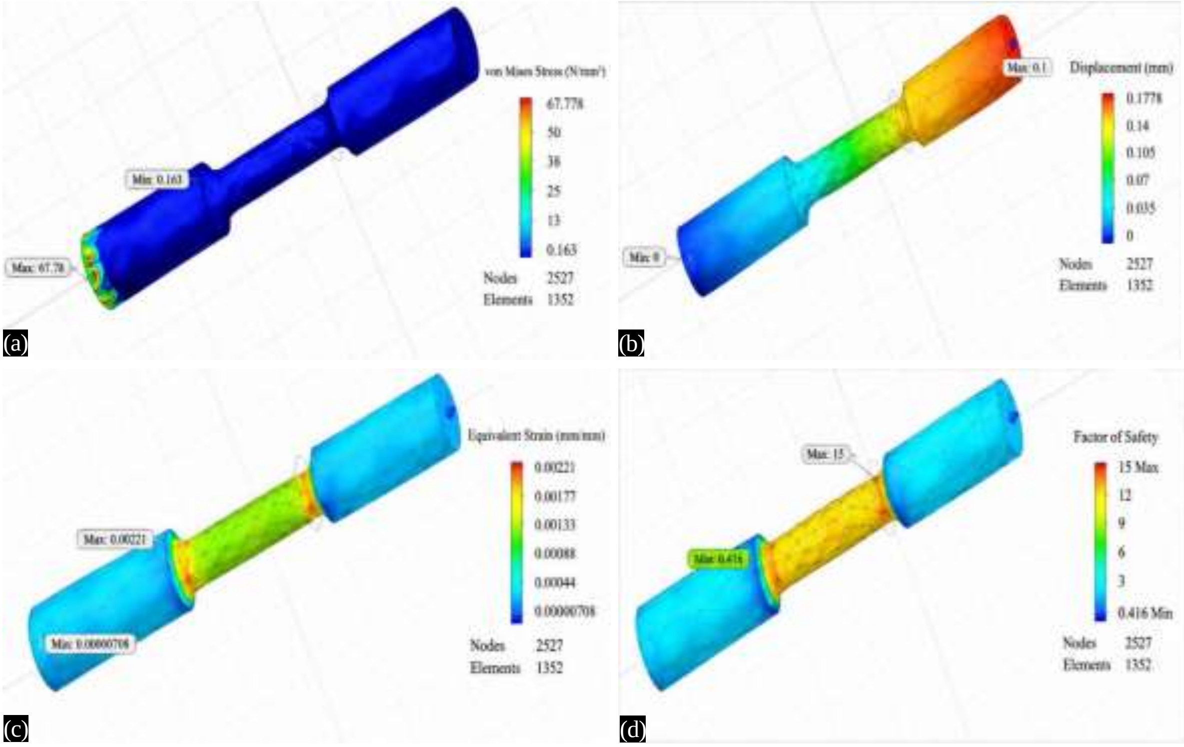

Figure 12. FEA simulation of Specimen 3. (a) reaction force; (b) displacement; (c) strain; (d)stress.

CONCLUSIONS

This study conducted a comprehensive investigation of Al6061-SiC metal matrix composites fabricated by stir casting at three SiC reinforcement levels (5%, 7.5%, 10%). The following principal conclusions are drawn:

1. Al6061 reinforced with 7.5 wt.% SiC (Specimen 2) exhibited the best overall mechanical properties: UTS of 137.44 N/mm², yield strength of 87.73 N/mm², and elongation of 6.18%, demonstrating an optimal balance of strength and ductility at intermediate reinforcement fraction.
2. Brinell hardness was highest for the 5% SiC composite (BHN = 68), while Charpy impact toughness was significantly reduced at 10% SiC (2 J vs. 4 J), indicating trade-offs between particle reinforcement density and dynamic toughness.
3. Optical microscopy revealed most uniform grain distribution for the 7.5% SiC specimen, with SEM confirming adequate particle-matrix bonding across all compositions. Higher SiC content (10%) led to particle agglomeration, explaining the observed reduction in ductility.
4. Taguchi L9 experimental results identified feed rate as the dominant parameter influencing resultant cutting force, contributing over 53% of total variance for the 5% SiC composite. Depth of cut-feed interactions became increasingly significant at higher SiC fractions (7.5% and 10%).
5. High-fidelity regression models ($R^2 > 91\%$) were developed for cutting force prediction at all three SiC fractions. These models provide practical tools for process planning and optimization of turning operations on Al6061-SiC composites.
6. FEA simulation corroborated experimental tensile results with good accuracy, confirming maximum stress of 171.2 MPa for the 7.5% SiC specimen and validating the chosen material models and boundary conditions.

The Al6061-7.5%SiC composite is recommended for applications demanding high specific strength combined with good machinability, including aerospace structural elements, automotive components, and marine engineering parts. Future work should investigate the effect of particle size distribution, heat treatment (T6 temper), and higher SiC fractions on both mechanical and machinability performance, and explore coated tool materials to further reduce cutting forces and tool wear.

- *Funding:* This research received no specific grant from any funding agency in the public, commercial, or not-for-profit sectors.
- *Conflicts of interest:* The authors declare no conflict of interest.
- *Data availability:* The raw data supporting the conclusions of this article will be made available by the authors upon reasonable request.

REFERENCES

1. Sharanya Nair, Nehal Joshi, "Preparation of Al 6061/SiC Metal Matrix Composite (MMC) using stir casting technique," International Journal of Engineering Research and Applications, vol. 1, no. 3, 2015.
2. Rajesh Agnihotri, Santosh Dagar, "Mechanical properties of Al-SiC metal matrix composites fabricated by stir casting route," International Journal of Advanced Research, ISSN: 2576-8816, 2017.
3. Ch. Hima Gireesh, K.G. Durga Prasad, Koona Ramji, "Experimental investigation on mechanical properties of an Al6061 hybrid metal matrix composite," Journal of Composites Science, vol. 2, 2018.
4. Revanasidappa M.D., Venkatesh K.C., Naveen C.R., "Mechanical and wear behaviour of Al6061-SiC-Gr hybrid composites," International Journal of Engineering Trends and Technology, ISSN: 2231-5381, 2016.
5. S. Gajanana, B. Suresh Kumar Reddy, A. Krishnaiah, "Analysis of machinability on Al6061 using single point cutting tool," International Journal of Scientific and Engineering Research, vol. 8, no. 4, 2017.
6. S. Gajanana, B. Suresh Kumar Reddy, A. Krishnaiah, "Linear model for turning Al6061 using Least Absolute Shrinkage and Selection Operator (LASSO)," International Journal of Scientific and Engineering Research, 2017.
7. Rama Rao S., Padmanabhan G., "Application of Taguchi methods and ANOVA in optimization of process parameters for metal removal rate in electrochemical machining of Al/5%SiC composites," International Journal of Engineering Research and Applications, vol. 2, no. 3, pp. 192-197, 2012.
8. N. Senthilkumar, T. Tamizharasan, V. Anandakrishnan, "Experimental investigation and performance analysis of cemented carbide inserts using Taguchi based grey relational analysis," Measurement, vol. 52, pp. 54–64, 2014.
9. Kapil Sharma, Dalgobind Mahto, S.S. Sen, "In metal turning, influence of rake angle on cutting tool life," International Journal of Application or Innovation in Engineering & Management, vol. 2, no. 8, 2013.
10. T. Tamizharasan, N. Senthilkumar, "Numerical simulation of effects of machining parameters and tool geometry using DEFORM-3D: Optimization and experimental validation," World Journal of Modelling and Simulation, vol. 10, 2014.
11. V.G. Aswathy, Dr. N. Rajeev, "Optimization in turning of Ti-6Al-4V using ANOVA and regression analysis," International Journal for Research in Applied Science & Engineering Technology, vol. 3, no. 9, 2015.
12. Renjith V.B., Mathew Baby, K.R. Jayadevan, "Influence of process parameters on cutting forces and Taguchi based prediction of T42-CT H.S.S single point cutting tool deflection," International Journal of Scientific and Research Publications, vol. 3, no. 7, 2013.
13. Krishankant, Jatin Taneja, Mohit Bector, Rajesh Kumar, "Application of Taguchi method for optimizing turning process by the effects of machining parameters," International Journal of Engineering and Advanced Technology, 2012.

14. M. Asad, F. Girardin, T. Mabrouki, J.-F. Rigal, "Dry cutting study of an aluminium alloy (A2024-T351): A numerical and experimental approach," International Journal of Machine Tools and Manufacture, vol. 53, no. 1, 2013.
15. W.T. Foster, "Basic Taguchi design of experiments," National Association of Industrial Technology Conference, Pittsburgh, 2000.
16. Samruddhi Rao, Pragati Samant, Athira Kadampatta, Reshma Shenoy, "An overview of Taguchi method: Evolution, concept and interdisciplinary applications," International Journal of Scientific and Engineering Research, 2013.
17. Ranganath M.S., Vipin, R.S. Mishra, "Optimization of surface roughness and material removal rate on conventional dry turning of aluminium (6061)," International Journal of Advance Research and Innovation, vol. 1, pp. 62–71, 2014.
18. Sijo M.T., K.R. Jayadevan, "Analysis of stir cast aluminium silicon carbide metal matrix composite," Procedia Technology, International Conference on Emerging Trends in Engineering Science and Technology (ICETEST), 2015.
19. P. Subramanya Reddy, "Investigation of mechanical properties of Aluminium 6061-Silicon carbide, Boron carbide metal matrix composite," International Journal of Mechanical Engineering and Technology, vol. 9, no. 2, 2018.
20. H. Bil, "Simulation of orthogonal metal cutting by finite element analysis," Master thesis, The Middle East Technical University, August 2003.
21. Qingchun Zheng, Cilei Yang, "Simulation and experimentation research on cutting force of turning titanium alloy," MATEC Web of Conferences, published by EDP Sciences, 2015.
22. ASM Handbook, Volume 2: Properties and Selection: Nonferrous Alloys and Special-Purpose Materials, 10th ed., American Society for Metals, 1990.
23. Schey, A.J., Introduction to Manufacturing Processes, McGraw-Hill, Singapore, 1987.

